Effect of Surface Roughness on Cyclic Ductility of Corroded Steel

Steve Burke[1] and Michel Bruneau, F.ASCE[2]

Abstract: Stable cyclic hysteretic behavior is required from structural members to dissipate seismic energy. Limited knowledge exists on the hysteretic behavior of corroded steel, and a relationship that quantifies energy dissipation capacity as a function of section thickness and roughness does not exist. Monotonic and cyclic tests of corroded steel were conducted in this research in an attempt to provide such quantification. Results from coupons suggest that assessing the strength of rusted members by machining a smooth coupon from steel extracted from an existing corroded structure, and only using the resulting yield and ultimate strength values in otherwise standard multilinear monotonic models, may be an unconservative approach. Results from cycling tests show that: (1) rusted steel can exhibit a significant hysteretic energy capacity, (2) a linear relationship exists between the total dissipated energy normalized by mean thickness and the mean 10-point-height of irregularities, and (3) increases in roughness correspond to decreases in the magnitude of total normalized energy dissipated before complete failure. **DOI: 10.1061/(ASCE)ST.1943-541X.0001425.**

Author keywords: Steel; Corrosion; Seismic; Ductility; Cyclic loading; Hysteretic energy; Surface roughness.

Introduction

Seismic evaluation of an existing steel bridge can be complicated when it is significantly corroded. Issues related to strength can be handled by standard procedures to account for section loss (e.g., Fisher et al. 1991; Kayser and Nowak 1989; Kayser et al. 1987; Kulicki et al. 1990), but issues related to cyclic ductility are typically neglected. Although uniform corrosion acts over large areas of steel and causes a decrease in cross-sectional area of structural members (accounted for in strength calculations), pitting corrosion is more localized. Some studies have shown that the ultimate strength analytically obtained from detailed models considering pitting corrosion is practically similar to that obtained from simpler models with uniform corrosion of equivalent average thickness (e.g., Nakai et al. 2005, 2006), with the smallest cross-section area often governing strength (e.g., Paik et al. 2004). Yet, there exists a potential for the pits to act as stress raisers during cyclic loading, akin to notches present on the steel surface (Albrecht and Simon 1981; Yu et al. 2012; Rajabipour and Melchers 2013; Gucuyen and Erdem 2014).

In that perspective, fatigue can be considered a surface sensitive process, and the ability to withstand cyclic loading may depend on the roughness of the member's surface. The pitting that occurs during corrosion may act as stress raising notches and increase the surface stress levels beyond what would be expected at a given level of loading for a smooth material. Many researchers have developed relationships for the decrease in the allowable stress range as a function of increases in corrosion time and/or in depth of corrosion [e.g., Bill (1982) for 12% Chromium (Cr) and 2.0% NiCrMoV steels], generally reporting an asymptotic reduction leveling to constant values as corrosion exposure time or pit depth increases. This indicates that a significant loss of fatigue life rapidly occurs as pitting corrosion develops. However, this past research addressed highcycle fatigue, for applied stress ranges below the yield stress. By contrast, seismic design relies on inelastic response and requires large ductility capacities.

Therefore, in earthquake engineering applications, stable cyclic hysteretic behavior is required from structural members to dissipate the seismic energy, and low-cycle fatigue is more relevant. Questions often arise in the course of seismic bridge evaluations as to whether corroded steel can develop the cyclic ductility necessary for satisfactory seismic performance. A limited number of tests on corroded steel (Bruneau and Zahrai 1998) have shown that good hysteretic energy dissipation is possible, but only up to a certain point and in a way that could not be related to an analytical model. In particular, the surface roughness of the corroded surface was not quantified in those experiments. Such knowledge is still lacking, and is desirable in the seismic evaluation of steel bridges.

To overcome this limitation, it was decided to conduct cyclic tests on corroded steel taken from a decommissioned bridge to assess if the hysteretic energy dissipation capacity of steel under cyclic loading could be related to measured surface roughness and thickness of the corroded surface. Given the limited number of specimens available on which such cyclic testing could be conducted, and in light of uncertainties regarding the appropriate method that should be used to measure thickness and whether the density of such measurements could affect the findings, a preliminary set of monotonic tests were conducted using simple tension coupons having corroded surfaces and taken from the same bridge. To compare the effectiveness of the various methods considered to measure thickness in these simpler preliminary tests, the data were used to develop finite element models to assess the ability of models having various resolution (and thickness mapping) to replicate the experimentally-obtained monotonic force displacement curves of the corroded steel. Incidentally, these monotonic tests also allowed determining how effective such finite element analyses can be when such models are constructed on the basis of only limited knowledge of material properties (a common condition encountered when performing evaluation of existing bridges).

[1]Professional Engineer, 219 Edgewater Rd., Sudbury, ON, Canada P3G 1J8. E-mail: Stephen.Burke2014@gmail.com

[2]Professor, Dept. of Civil, Structural, and Environmental Engineering, Univ. at Buffalo, NY 14260 (corresponding author). E-mail: bruneau@buffalo.edu

Note. This manuscript was submitted on December 21, 2014; approved on August 25, 2015; published online on January 19, 2016. Discussion period open until June 19, 2016; separate discussions must be submitted for individual papers. This paper is part of the ***Journal of Structural Engineering***, © ASCE, ISSN 0733-9445.

Findings from this limited monotonic and cyclic testing program are presented in this paper, with the understanding that the primary objective is to investigate the ductile behavior of corroded steel under cyclic loading as a function of measured surface roughness and thickness of the corroded surface.

Preliminary Monotonic Tests

As mentioned previously, monotonic tests were conducted to investigate which method should be used to measure thickness and whether the density of such measurements (as gauged by the ability of finite element models to match experimental results) could affect the findings in subsequent cyclic tests. To determine the best approach to measure the thickness of corroded steel members, various methods were used to quantify the thickness of five corroded lacing bars taken from the built-up members of a decommissioned corroded steel bridge constructed in the 1950s. The lacing bars were machined from their original dimensions down to standard ASTM long-tension test specimens (ASTM 1991), but leaving the two corroded 38.1- mm wide sides of the specimens in their original corroded condition [as shown in Fig. 1(a)]. These specimens were then vigorously cleaned with a wire brush to remove any loose scale. The surface of the lacing bar's 203.2- by 38.1-mm test area was then divided into a 6.35- × 6.25-mm grid for testing, resulting in a fine grid of 6 spaces wide by 32 spaces long [Fig. 1(b)]. This grid size was chosen to match the anvil size of the screw micrometer and the smallest ultrasonic transducer used to measure thickness. The specimens showed varying degrees of corrosion over their lengths with some portions of the lacing bars being only approximately half the thickness of sections on the same lacing bars that were located only a few inches away. The various testing methods considered are described subsequently.

Thickness Mapping

Each specimen was first measured using a standard micrometer with (1) no anvil attachments, (2) a 5.08- mm diameter ball tip, (3) a 0.991-mm diameter comparator tip, and (4) a 1.981-mm diameter spline attachment for a total of four grids of 192 readings per grid, or 768 thickness measurements per specimen. The results were reviewed every 64 readings (two full rows of readings), and suspect results were double checked. Although the micrometer itself is an inexpensive instrument, data collection is time consuming (at least 30 s per data point, or 205 h of work per 1 m^2 of steel if using the grid spacing used in this research). Beyond possible errors from operator fatigue, a tilting error also may induce errors (quantified in Burke and Bruneau 2002).

Specimens were then measured using ultrasonic testing, first using a Parametric Epoch (Olympus NDT Canada, Québec, Canada) III flaw detector and a 6.35-mm (0.25 in.) diameter transducer, calibrated using blocks of various thicknesses (3.81, 6.35, and 8.89 mm) machined smooth from the same material as the corroded steel. However, once the transducer was placed on the test coupon, it became immediately apparent that the ultrasonic wave was not performing in the same manner as it had when the flaw detector was being calibrated. Results displayed an erratic array of multiple responses and moving peaks with no obvious back wall echo, possibly attributed to the fact that many portions of both corroded surfaces of the test coupons were not perpendicular to the incident sound waves, coupled with the fact that the wear face of the transducer often was not horizontally stable on the surface of the material because of the irregular rusted surface.

As an alternative approach, a depth meter (D-meter) was used, as this device was deemed better suited to this problem. The main advantage of the D-meter is that built-in controls interpret the returning signal for the operator and display it numerically. An older-model, Wylam Hill Portable D-meter (Coltraco, New York), was used, and initially calibrated (as described previously) and recalibrated after every 64 readings (every two rows) to ensure accuracy of the results. Most of the readings were obtained in approximately 10 s, giving the operator a chance to stabilize the transducer over the grid location and record the reading (corresponding to 70 h of work per 1 m^2 of steel for the grid spacing used). Many newer D-meters have data storage capabilities that can decrease the time required for testing.

Many of the problems that occurred during the use of the flaw detector most likely occurred to some degree when the D-meter was being used, but suspect readings were compared to those recorded by the screw micrometer; if found to be far different, the readings were taken anew. If the repeated measurements did not differ from the original, they were recorded as displayed on the D-meter.

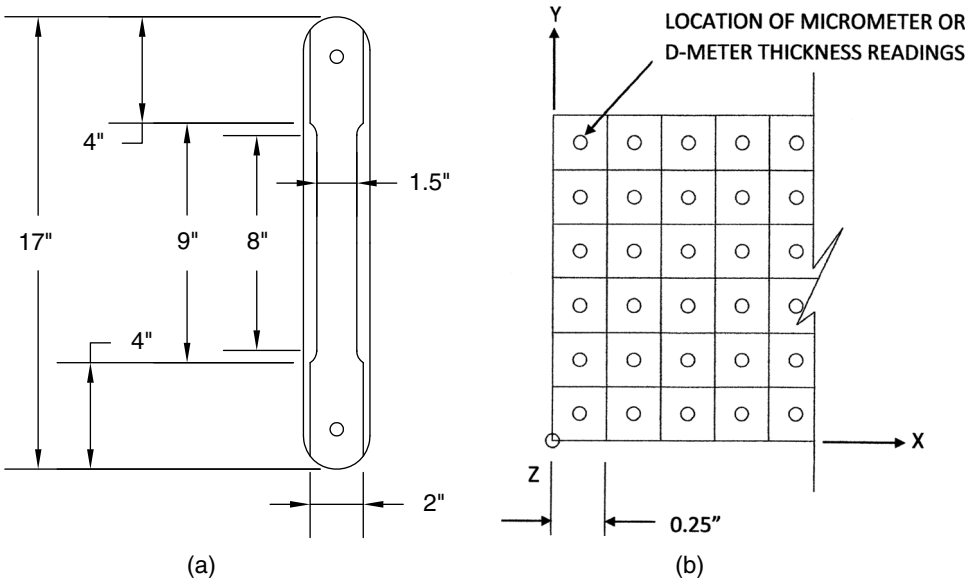

Fig. 1. Monotonic test specimen: (a) dimensions of specimen cut out of lacing bar; (b) grid of thickness measurements

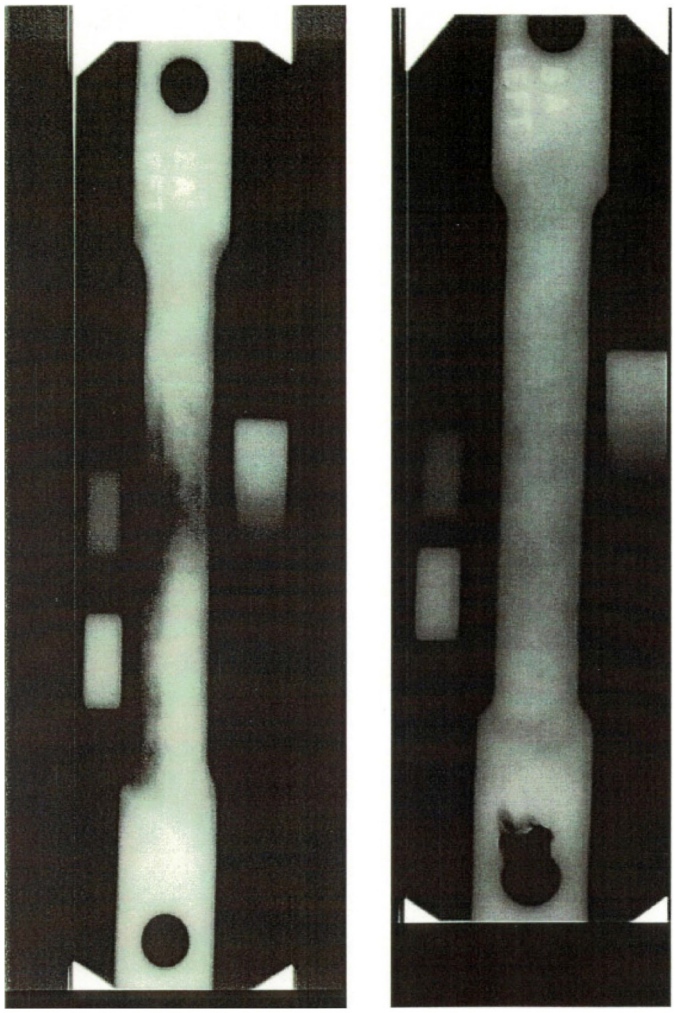

(a) (b)

Fig. 2. X-ray images of monotonically tested: (a) specimen 1; (b) specimen 5

During the conduct of this project, the authors had the opportunity to sample ultrasonic testing using an air-coupled micromachined capacitance transducer (courtesy of the Non-Destructive Testing Group of the Aerospace Research Institute at the National Research Council, Ottawa, Ontario). The procedure allowed testing a specimen in only a few minutes, focused onto surface points as small as 200 μm, and through transmission thickness readings possibly accurate to within ± 5 μm of total thickness, but the procedure could not be used in this project.

In an attempt to illustrate thickness mapping, X-ray images of the specimens (together with sloped wedges machined from the same material and placed next to the specimen to serve as thickness references) were taken by a Canadian General Standards Board (CGSB)-certified level II technician from a commercial inspection service; although the images (shown in Fig. 2 for Specimens 1 and 5) could not be digitized because of radiation burn-through and other issues, they provide qualitative information on thickness variations across the specimens.

Summary of Thickness Results

Mean, median, mode, skewness, kurtosis, variance, standard deviation, standard error, range, maximum, and minimum of the data collected by each method are presented in Burke and Bruneau (2002). For the current purpose, key information is summarized as follows:

- Histograms indicated that the data generally followed a normal distribution, except for the data recorded using the D-meter for two of the five specimens that exhibited a second smaller peak (it could not be determined with certainty if this slightly bimodal behavior was because of internal laminations in the specimen causing the wave to rebound at approximately half the full thickness of the specimen, or to the inherent difficulty of recording thickness measurements of a corroded surface using ultrasonic techniques).
- The arithmetic means, calculated medians, and modes for the data collected for the thickness mapping were all of a similar magnitude, although the results obtained using the D-meter differed by roughly 10% from the sets of data recorded using the screw micrometers when the previsouly mentioned bimodal behavior was observed in the D-meter data.
- With respect to variance, standard deviation, and standard errors, the results obtained from the screw micrometer were within the same order of magnitude, and the results from the D-meter were more scattered.

Tension Tests

Following the thickness evaluation of the specimens, the five corroded specimens, together with a smooth control specimen, were subjected to tensile testing. The control specimen was a standard ASTM (1991) long-test specimen of identical shape (i.e., 203.2-mm gauge length and a 38.1-mm gauge width), machined to remove all corrosion products. For illustration purposes, the resulting force displacement curves are shown in Fig. 3 for Specimen 1, and in Fig. 4 for Specimen 5. The difference in results reflects the fact that differently corroded specimens, even though of same steel material, will behave differently as a consequence of their different corrosion patterns (i.e., varying thicknesses and roughness along the length of the specimen). Results are presented in terms of force-versus-displacement; results in terms of stresses and strain would not be meaningful except for the smooth control specimen because of the varying cross-section of the corroded specimens. Yield strength values ranged from a low of 56.6 kN to a high of 84.6 kN, and ultimate strengths ranged from a low of 79.8 kN to a high of 121.6 kN for the five corroded specimens. The control specimen had yield and ultimate strengths of 114.35 and 162.64 kN, respectively.

Displacements in the force-displacement curve for Specimen 5 were only recorded up to approximately 2 mm because the 203.2-mm long extensometer was removed shortly after the yield point, and the required data from yield to final rupture was not obtained (contrary to Specimen 1, for which the extensometer was only removed at approximately 8 mm; also, results are not presented for Specimens 2, 3, and 4 because the extensometer was removed prematurely in those cases). However, the data from Specimen 5 are useful for the subsequent comparisons, and to confirm the absence of a sharp transition from the elastic to plastic range [which is consistent with what was observed by Bruneau and Zahrai (1998), and attributed to the variable cross-section because of the irregular material loss due to corrosion].

Although the control specimen fractured at an elongation of 27%, by comparison, Specimens 1 through 5 fractured at elongations of 5, 16, 10, 18, and 15%, respectively. Considering that the dividing line between brittle and ductile materials is sometimes defined as 5% elongation at failure (Fitzgerald 1967), this suggests that Specimen 1 could be considered a minimally ductile material even though the original noncorroded structural steel was most

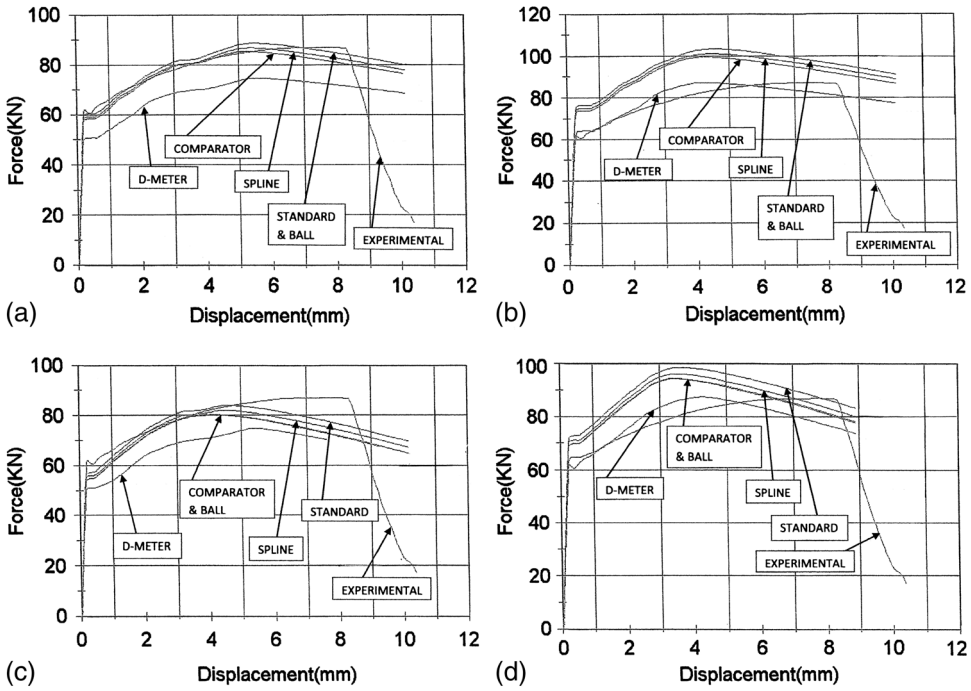

Fig. 3. Force displacement curves for specimen 1 (reprinted from Burke 2002): coarse mesh results in (a) and (b); fine mesh results in (c) and (d); specified materials properties in (a) and (c); coupon materials properties in (b) and (d)

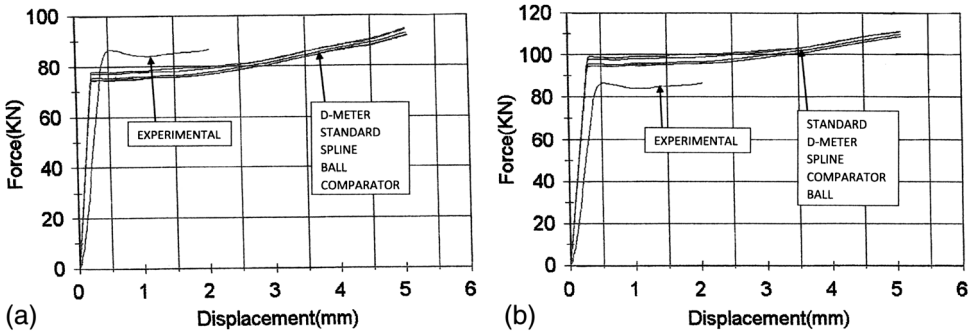

Fig. 4. Force displacement curves for specimen 5, fine mesh using: (a) specified material properties; (b) coupon material properties [(a) and (b) reprinted from Burke 2002]

certainly ductile. This could be a consequence of corrosion pits being stressed to an increased level, leading to crack initiation and redistribution of the applied forces to cross-sections of lower area.

Finite Element Modeling

To investigate the quality of the nondestructive thickness mapping, finite element modeling was performed for the five specimens. Each of the five specimens was mapped using five measurement methods, resulting in a total of 25 thickness maps. For each of the thickness maps, two geometric and two material property model variations were investigated.

The first geometric model used all of the thickness data collected to construct a fine mesh geometric model. The second geometric model was constructed to determine if there was a loss of finite element analysis accuracy if fewer thickness readings were recorded during the nondestructive testing. The fine and coarse geometric models were both analyzed using each of the two previously mentioned material property models. Models were constructed using the *ANSYS* computer program. Meshing was accomplished using 8-node "SOLID 45" elements from the *ANSYS* element library, which are able to model large deformations and large strains. The fine and coarse mesh models had 231 and 85 elements, respectively. Both models were created from the 192 thickness readings that were recorded using the five previously mentioned nondestructive evaluation methods, namely the four micrometer thickness grids and a depth meter grid (assuming all midthickness points to lie on the same plane). As such, the coarse mesh investigated the consequence on accuracy of using only half of the available thickness readings.

Two different material models were used in the finite element analyses conducted in attempts to replicate the experimentally obtained force-displacement curves. In the first case, the yield and ultimate strengths obtained from the tensile testing of the smooth control specimen were used to construct a quadrilinear model of the

material's behavior. In the second case, a similar quadrilinear stress-strain curve was built using the specified yield stress and ultimate stress of 248.2 MPa (36.0 ksi) and 381.3 MPa, respectively, taken from the "American Institute of Steel Construction Handbook for Iron and Steel Beams from 1873 to 1952" (AISC 1953) for A7 bridge steel from the 1950s. In both cases, elastic and shear moduli of 200,000 and 77,000 MPa were respectively used, along with a Poisson's Ratio of 0.3, and the onset of strain hardening was assumed to occur at 15 times the yield strain, with a strain hardening modulus equal to E/30 (Bruneau et al. 2011). This allowed investigating the fidelity of simulations when analyses are built with only that limited knowledge (as is often the case in bridge engineering practice).

Finite Element Results

From resulting force-displacement results presented in Figs. 3 and 4 (results cannot be presented in terms of stresses and strain because of the varying cross-section of the corroded specimens), it is shown that the finite element modeling results obtained from the five measurement techniques are essentially similar, being within approximately 5% of each other along the full length of the curves; the only exception to this being the D-meter results for Specimen 1, which are approximately 15% lower overall (for reasons described previously).

Also seen in those figures, in terms of the finite element models' accuracy in matching the actual tensile testing results, the models using specified A7 properties generally produced slightly conservative results. However, when using the control specimen's actual yield stress of 315.1 MPa and ultimate stress of 448.2 MPa, as material properties in the finite element analyses, the yield and ultimate forces of the corroded specimens were overestimated by approximately 25%. It also is observed that for Specimen 1, the peak strength was reached at a smaller displacement for the fine mesh cases than for the coarse mesh and actual coupon tests; although this is not of importance in this study, it may warrant further attention in future studies.

In most cases, as shown in Figs. 3 and 4, the mean difference between the analytical results obtained for the fine and coarse geometric models was less than 5%. Finally, the difference between the finite element and tensile testing results past the ultimate strength is not of concern because the abrupt experimental drop seen in the figure is only there because no data were recorded beyond that point, and a line was drawn down to the final elongation point measured by putting the ruptured pieces together. The finite element models also did not account for cracking and fracture, making comparison beyond the ultimate strength a moot point. However, note that if finite element analysis had been used to predict fracture, it is possible that mesh size could have had a significant effect on the results (although this is beyond the scope of the current study and was not investigated here).

Cyclic Testing–Out-of-Plane Bending of W-Shape Web

Description of Specimens

As indicated previously, the objective of this research was to investigate if the cyclic ductile response of corroded steel under repeated cyclic inelastic loading could be related to measured surface roughness and thickness of the corroded surface. For this purpose, specimens were extracted from two long segments of wide-flange beams flame-cut from a 1950s Warren truss bridge demolished in the 1990s. The first was an end crossbeam and the second was an interior crossbeam, originally specified on the drawings as 24-in. wide flange (WF) @ 80 and 27-in. WF @ 91 structural shapes, respectively. These beams were selected because they were representative of the various levels of corrosion present on that bridge, and because they allowed use of a convenient test setup to apply a cyclic displacement regime to the corroded steel.

To allow controlled testing in the laboratory, the specimens were prepared as smaller sections cut from the beams using a band saw. In total, four samples were prepared for the cyclic tests conducted during this stage of the research, namely two 267-mm long 27-in. WF @ 91, one 356-mm long 27-in. WF @ 91, and one 356-mm long 24-in. WF @ 80. The ends of the four specimens were then ground smooth to remove any small defects or notches that may act as stress raisers during the cyclic testing of these samples.

Experimental Set-Up

The experimental setup used for the cyclic testing was not intended to replicate the actual seismic effects that would occur on the bridge beams during an earthquake, but rather to provide a convenient setup to subject the WF sections to cyclic weak axis bending at their most corroded cross-section, namely the web near flange-to-web intersection. As shown in Fig. 5, bolts located as close as possible to the web of the W-shape specimen were used to connect the flange of that W-shape to a rigid steel base, itself anchored to the strong floor. Six bolts (three on each side of the web) were used for this purpose. This positioning of the bolts was chosen to effectively eliminate the potential effect of flange flexure on the rotation of the specimen.

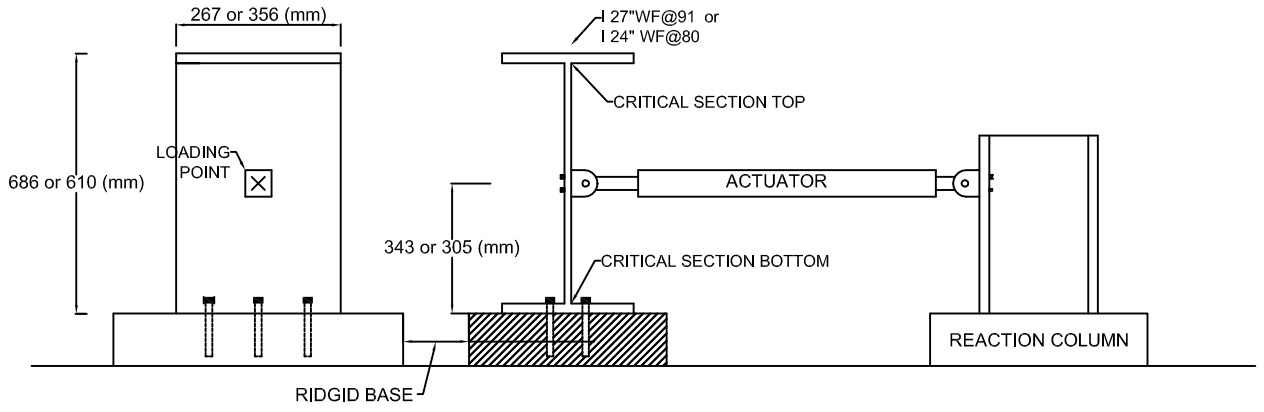

Fig. 5. Experimental setup

The setup consisted of a strong reaction column, a rigid base, and a small hydraulic actuator (with a maximum loading capacity of 25 kN) connected at midheight of the web, as shown in Fig. 5, and used to cycle the cantilevering web in flexure about its weak axis. This allowed testing the most severely rusted portion of the W-shape's web, namely near the web-flange intersection. Connecting the actuators at midheight of the web allowed flipping the specimen to conduct two tests per specimen. After the first test on each specimen, instrumentation and actuator were removed, the specimen was flipped over and reconnected to the rigid base, and the next test was conducted. As such, Tests 1 and 2 are on Specimen 1, Tests 3 and 4 are on Specimen 2, and so on, sequentially testing the web near both web-flange intersection points.

Instrumentation of the specimens included a load cell and LVDT internal to the actuator, and four external LVDTs. The internal load cell and LVDT were used to monitor the applied loading and displacement of the specimen. Two of the external LVDTs were used to monitor rotation of the web-to-flange intersection (found to be negligible), and the final two external LVDTs were used to determine if any slippage was occurring between the rigid base and the concrete floor, and between the specimen and the rigid base (both also found to be negligible).

Thickness and Roughness Measurements

Before cyclic testing of the specimens could begin, thickness and roughness measurements were recorded. Based on the results of the finite element modeling, a micrometer with no anvil attachment and a measurement grid spacing of 12.7 mm were selected for the thickness mapping. Each specimen was vigorously cleaned with a wire brush before measurements were taken. Given that it was expected that failure would eventually occur near the bottom of the W-shape web, but impossible to predict exactly where (as thickness and roughness varied locally there), either three or four rows of thickness were measured along the length of each web, starting at the middle of the bottom web-to-flange intersection, up to a point between 38.1 and 50.8 mm along the height of the web from that bottom flange. Thickness results at the location at which fracture eventually occurred are presented in a subsequent figure, but as a preliminary indication of the extent of rusting over all the lines sampled, Specimen 1 to 4, respectively, had an average thickness of 11.04, 6.94, 10.06, and 10.32 mm (dropping to lows of 9.53, 4.65, 5.87, and 8.50 mm, respectively). The original (i.e., not corroded) web thickness of Specimens 1, 3, and 4 (27 WF @ 91 sections) was 12.3 mm, and Specimen 2 (24 WF @ 80 section) was 11.6 mm.

Roughness was measured using Testex (Newark, Delaware) replica tapes (Testex Corporation 1999), which typically consists of a layer of crushable microfoam (available in various thicknesses) coated onto 50 μm of an uncrushable plastic backing film. Firm pressure is applied uniformly over the back of the replica tape by a special burnishing tool, to crush the microfoam on the surface to be measured. Removing the tape from the surface provides a reverse replica that can be measured using a variety of methods.

To eliminate all small corrosion debris that could corrupt the roughness readings, surfaces in which sampling was to be made were cleaned using a solution obtained by mixing 500 mL of hydrochloric acid, 3.5 g of hexamethylene tetramine, and distilled water to make a total of 1,000 mL of cleaning solution, and applied for 10 min at 20 to 25°C per wash [per ASTM G1-90 (ASTM 1999) "Standard Practice for Preparing, Cleaning, and Evaluating Corrosion Test Specimens," Table Al for cleaning of iron and steel]. Four washes were required to remove 95% of the corrosion product, based on findings from cleaning tests conducted on smaller specimens that could be weighted between washes. To avoid having to submerge the entire WF section into the solution, a 75-mm long 100-mm diameter section of PVC pipe was sealed to the web using window putty, and the cleaning solution was poured into the pipe. The procedure resulted in a 100-mm diameter circular area in which the corrosion product was removed. Although new thicknesses could have been measured at the locations in which enhanced removal of corrosion was achieved chemically, this would have led to inconsistency in the thickness readings, with some values inside and outside of the chemically cleaned areas. Given that cleaning and roughness sampling of the entire cross-section to be tested was prohibitive, it was deemed more appropriate to only use the thicknesses measured as reported prior to cleaning. It also is consistent with the expected site conditions in practical applications in which chemical cleaning over large surfaces for the purpose of performing the Testex replication procedure (described previously) is unlikely to be done.

Three replica tape samples were taken at representative locations at which thickness measurements had been taken on the web, near each flanges of each specimen, and on each side of the web, for a total of 48 extra coarse plus replica tape samples. These samples were then sent to Testex in Newark, Delaware, for roughness quantification using a Mitutoyo replica tape (Mississauga, Ontario) thickness gauge to obtain a mean 10-point-height of irregularities roughness. Although this is the only roughness parameter that the Mitutoyo replica tape thickness gauge is capable of recording, it is an accepted indicator of surface roughness. The Structural Steel Painting Council (SSPC), ASTM, and the National Association of Corrosion Engineers (NACE) all use this parameter. The average 10-point-height of irregularities roughness values measured ranged from a low of 99 μm to a high of 185 μm, with an overall average value of 145 μm. Specimen 1 had the least amount of surface roughness with a mean value of 136 μm, followed by Specimens 3, 4, and 2 with mean values of 138 μm, 148 μm, and 159 μm, respectively. With respect to the eight tests performed, the surface for Test 2 possessed the lesser roughness, followed by Tests 6, 7, 5, 1, 3, 8, and 4, with mean roughness values of 131 μm, 137 μm, 137 μm, 139 μm, 140 μm, 153 μm, 158 μm, and 165 μm, respectively. This resulted in a maximum deviation from the mean of all values of 20 μm or 13.8%.

This approach retained for measuring surface roughness was found to be the most effective and practical for this study as a result of prior replication trials performed using various thicknesses of replicate tape, and prior trials to quantify roughness using alternative methods, namely: interpretation using a bright field illumination optical microscope (at the Fine Particle Research Lab in the Physics Department at Laurentian University, Sudbury, Ontario) at various magnification levels and fields of view; a scanning electron microscope (at the Geosciences Laboratory of the Geological Survey of Canada, Sudbury, Ontario) using gold coated replicate tape at 100X magnification and field-of-view of approximately 0.8 mm; optical interference microscope (performed by both the Zygo Corporation, Middlefield, Connecticut and Veeco Metrology) at various magnifications; and readings using the Mitutoyo replica tape dial gauges (performed by Testex).

Experimental Results: Cyclic Response and Hysteretic Energy

Each of the eight tests began with a few test cycles that were used to determine the approximate yield displacement, Δy, for each member. Each specimen was subjected to an applied loading that pushed the specimen into the nonlinear range, and unloaded it to determine if there had been any residual deflections (indicating that

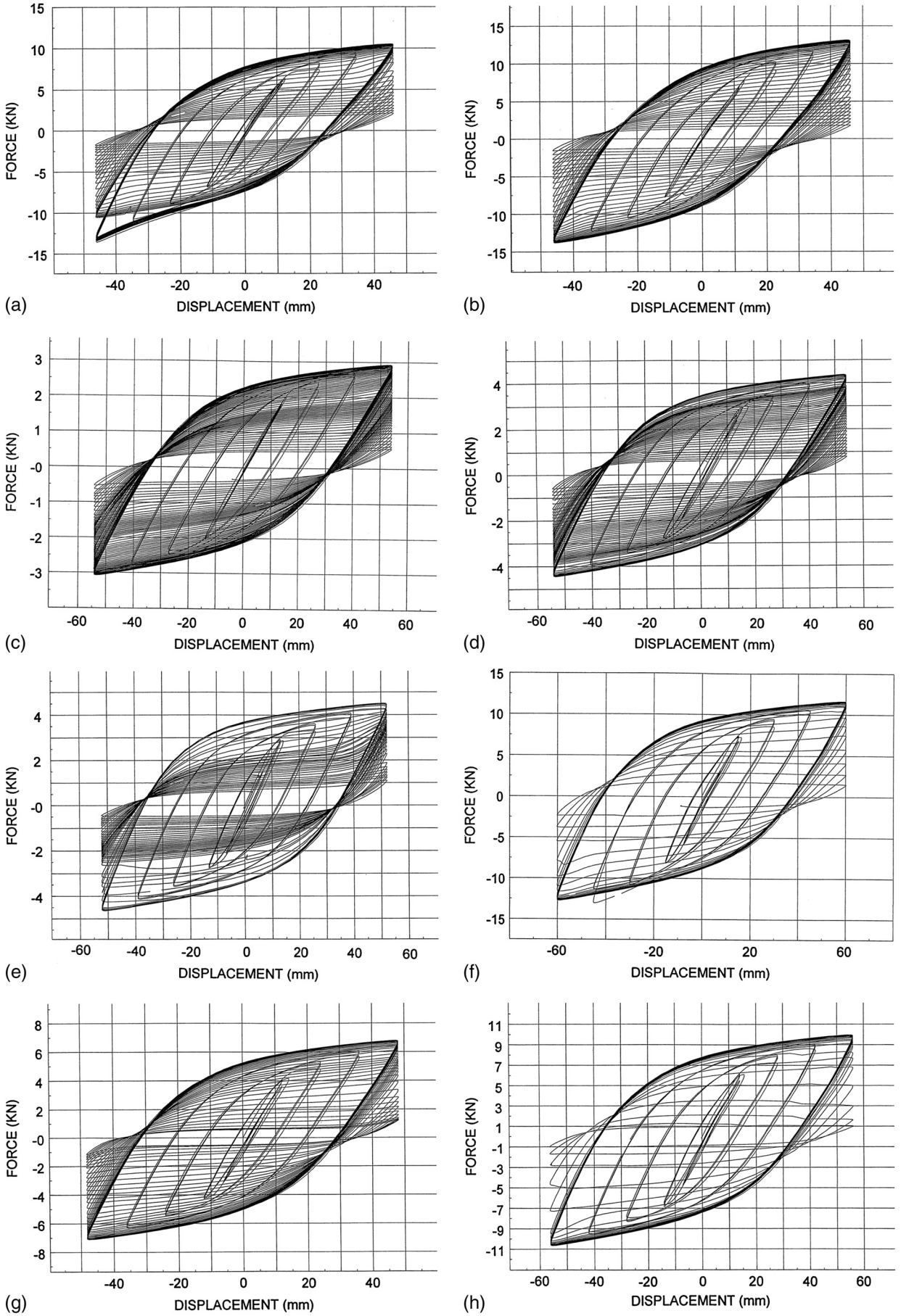

Fig. 6. Hysteretic curve results (reprinted from Burke 2002): (a) test 1; (b) test 2; (c) test 3; (d) test 4; (e) test 5; (f) test 6; (g) test 7; (h) test 8

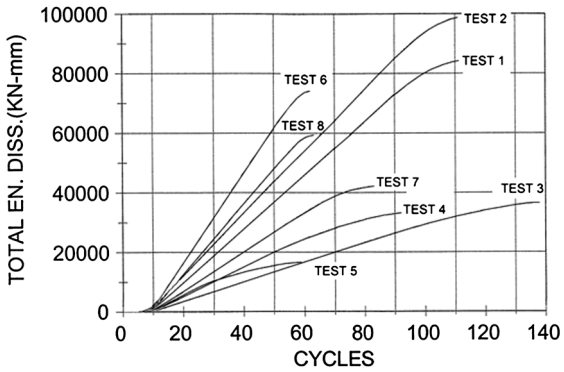

Fig. 7. Cumulative energy dissipation during cycling

the yield point had been exceeded). Although analytical calculation of the yield deflection was difficult to perform because of the varying cross sectional areas, it was rather defined to be at the approximate intersection points of lines drawn asymptotically from the nonlinear and linear portions of the force displacement curve.

Following this (i.e., after the yield deflection had been determined), the specimens were subjected to a preprogramed cyclic displacement history. The displacement history consisted of three cycles of $\pm 0.50\Delta y$, $\pm 1.00\Delta y$, $\pm 2.00\Delta y$, and $\pm 3.00\Delta y$, followed by cycling to failure at $\pm 4.00\Delta y$. The loading rate for all of the testing was 1.0 cycles/min, continued until the specimen's capacity decreased below approximately 20% of the maximum capacity. The corresponding hysteretic curves are shown in Fig. 6. The resulting cumulative energy dissipation per cycle for all eight tests is shown in Fig. 7.

From a purely qualitative assessment, the experimentally-obtained hysteretic curves suggest that ductility of the corroded steel considered in this study is substantial and most likely adequate to provide satisfactory seismic performance. More quantitatively, for comparison purpose, the AISC 341-10 Seismic Provisions' cyclic testing requirements for the qualification of buckling-restrained braces (AISC 2010) requires achievement of a cumulative inelastic deformation of at least 200 times the yield deformation for a buckling-restrained brace to be satisfactory (although that is demanded of buckling-restrained braces, many other structural systems commonly used to provide seismic resistance would not be able to develop such a large sustained ductile response). At a displacement ductility demand of $\pm 4.00\Delta y$, this cumulative plastic deformation value of $200\Delta y$ is achieved in 17 cycles (subtracting the elastic deformations from each cycle). In this study, all the corroded specimens tested underwent significantly more ductile cycles without strength degradation than required by this stringent qualification requirement (as shown in Figs. 6 and 7).

Throughout each experiment, the hysteretic curves were closely monitored for decreases in applied forces. If any such drop in strength was noticed, the cyclic testing was stopped and the specimen was inspected for signs of cracking. If cracks were found during the inspection, they were documented. For example, typical onset of cracking as observed during testing is shown in Fig. 8(a) (at the 80th cycle), and a representative significant crack propagation is shown in Fig. 8(b) (at the 92nd cycle). Mapping of the specimen thickness across its width along the line at which cracking occurred and locations of first observed cracks are shown in Fig. 9.

Unfortunately, laminations were found through the thickness of the web material for Tests 5, 6, 7, and 8. In several instances, these flaws seemed to have had damaging effects on the material's ability to dissipate energy. Internal laminations propagated toward the

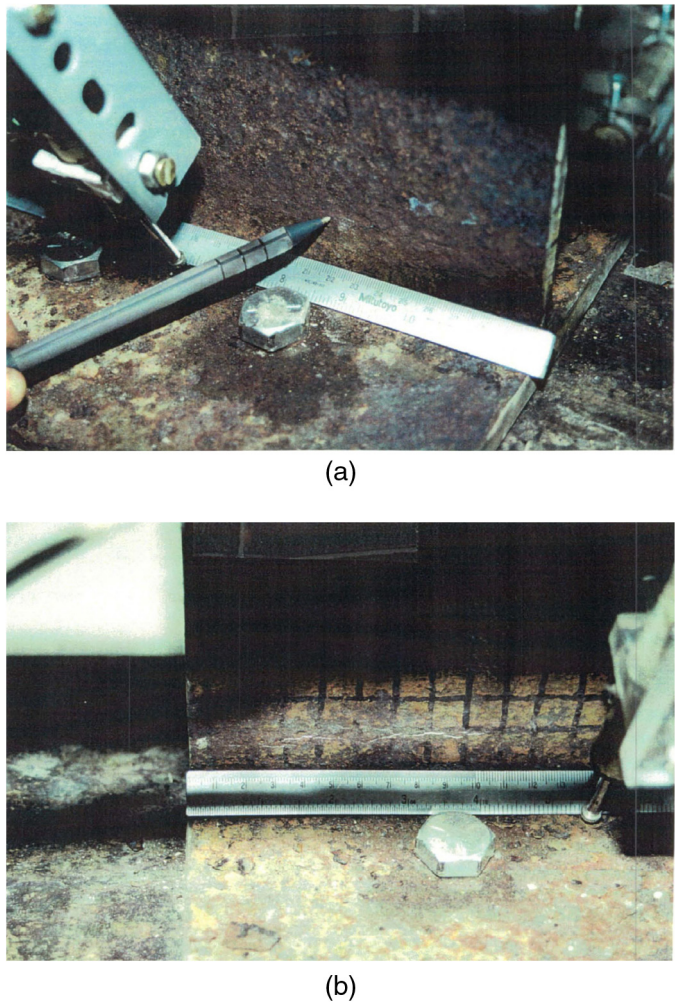

(a)

(b)

Fig. 8. Crack propagation in cyclic test 3: (a) hairline crack at 80th cycle; (b) Propagated crack and 92nd cycle

surface of the web material and joined with surface cracks during Tests 5 and 7, and remained internal for Tests 6 and 8. These internal laminations may have contributed to the premature failures noticed during several tests. The most detrimental example of the negative effect of an internal lamination upon the energy dissipation abilities of a material occurred during Test 5. This test exhibited stable hysteretic behavior to only the 24th cycle, at which point a loud popping noise was heard and a long tear was found on the web (Fig. 10).

Table 1 summarizes results from the nondestructive and cyclic testing performed on the eight corroded web-to-flange intersection points (Tests 1 to 8), in terms of assumed yield load and deflection, mean thickness, mean of the thickness readings from the area of initial cracking, visible crack location, lowest thickness value for the test area, mean 10-point-height of irregularities roughness for the north and south faces of the web, total energy dissipated, normalized dissipated energy, number of cycles to initial cracking, and number of cycles to failure. This information was used to compare the performance of the eight corroded webs (in the vicinity of their respective web-to-flange intersection points).

Preliminary Observations on Experimental Data

Data in Table 1 revealed that in almost all cases, mean thickness in the area of initial cracking was lower than the mean thickness

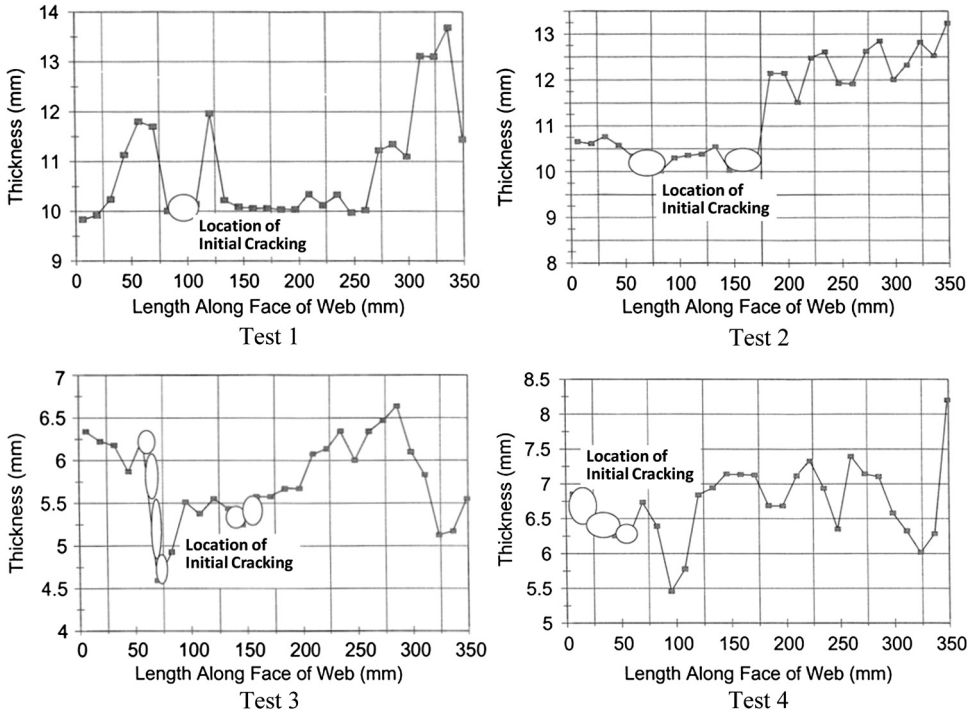

Fig. 9. Thickness across width of specimens, and location of initial crack observed (circled areas indicate locations of initial cracks)

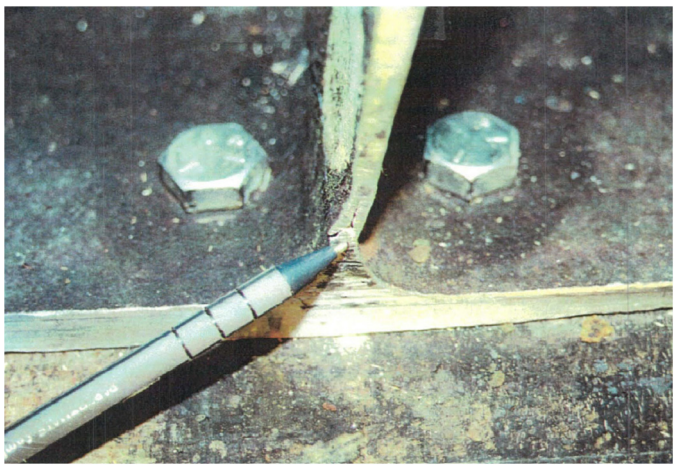

Fig. 10. Lamination observed in cyclic test 5 (shown at 30th cycle)

values for the entire area for a specific test. The only exception to this was Test 5, which failed abruptly at a low level of energy dissipation and low number of cycles (for reasons subsequently described). This indicates that low cycle fatigue, combined with the negative effects of corrosion induced surface roughness, have a more detrimental effect upon thinner, lower strain areas of the cross-section than they do upon the thicker, higher strained areas of the cross-section.

However, analysis of results indicated no consistent correlation between mean thickness, thickness at the location of initial cracking, low thickness and mean roughness, against total energy dissipated, normalized energy dissipation, and number of cycles to cracking and failure, except for the following observations:

- Specimens with smaller thickness (e.g., mean thickness, mean thickness at cracking, or lowest thickness over the test area) tend to dissipate less energy than thicker materials, but not in a discernable correlated manner.

Table 1. Summary of Cyclic Testing Data

Test number	P_Y (kN)	Δ_Y (mm)	t_{MEAN} (mm)	t_{CRACK} (mm)	t_{MIN} (mm)	Roughness (μm)	E_H (Total) (kN mm)	E_H (Norm.) (kN mm)	Cycles to cracking (#)	Cycles to failure (#)
1	6.37	11.5	10.51	10.02	9.53	140	84,312	1,151	86	112
2	7.00	11.5	11.56	10.17	10.02	131	98,844	1,228	82	112
3	1.83	13.5	6.41	5.42	4.59	153	36,701	1,486	72	139
4	2.58	13.5	7.47	6.48	4.65	165	33,227	954	52	82
5	2.88	13.5	8.72	10.6	5.87	139	16,804	449	24	59
6	7.38	15.0	11.84	11.26	11.17	137	74,342	672	42	61
7	4.00	12.0	9.44	9.11	8.5	137	42,200	879	52	83
8	6.00	14.0	11.20	11.14	10.78	158	59,376	707	52	64

Note: t_{MEAN} = mean thickness of all thickness readings for the web-to-flange intersection being tested; t_{CRACK} = mean thickness of the thickness readings located at which the first crack was noticed; t_{MIN} = lowest thickness reading that was recorded for the web-to-flange intersection being tested; roughness is the mean of the six 10-point height of irregularities roughness measurements taken for each web-to-flange intersection point; E_H (Total) = total energy that was dissipated during testing; EH (Norm.) = normalized energy that was recorded during testing. The total energy dissipated was normalized by the yield displacement (Δ_Y) and yield force (P_Y); cycles to cracking is the number of cycles between the beginning of testing to the point when cracking was first noticed; cycles to failure is the number of cycles from the beginning of testing to failure.

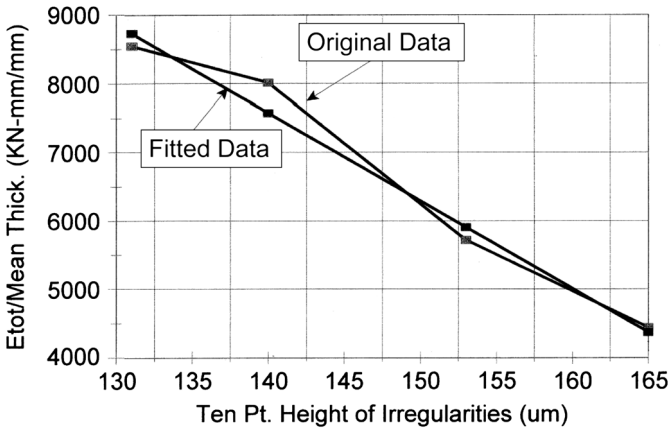

Fig. 11. Total energy dissipated normalized by mean thickness, versus 10-point height of irregularities roughness (original data and best fit linear curve)

- Specimens having lower mean 10-point-height of irregularities roughness tend to dissipate less energy than smoother materials, but not in a discernable correlated manner.

Correlation of Results with Roughness and Thickness

In subsequent analyses, based on close scrutiny of the obtained results, and some rational inferences, it was considered logical that both surface roughness and material thickness be interrelated in impacting energy dissipation capabilities of the specimens as follows. First, hysteretic energy of a rectangular cross section at yield (or at a fixed number of times the yield displacement) can be shown to be directly proportional to its thickness (considering the dependence of both M_p and Δ_y on thickness). This suggests normalizing energy dissipation by thickness for subsequent comparison. Second, it was deemed more appropriate to use mean thickness and mean ten-point-height of irregularity roughness in subsequent comparisons as these parameters are the least affected by human judgment.

Therefore, normalizing the total energy dissipated during Tests 1 to 4 by the mean thickness of the test area to obtain a theoretically constant value (for a rectangular section), and plotting that against the mean 10-point-height of irregularity values for the specific tests, it is shown in Fig. 11 that as the surface roughness values increase in magnitude, the material's ability to dissipate energy decreases in a significantly correlated manner. A straight line fitted to the data (using a least square method of curve fitting) resulted in the following equation:

$$Y = -128.2X + 25527$$

where Y = total energy dissipated normalized by the mean thickness of the material in units of kN-mm/mm; and X = measured value of the 10-point-height of irregularity surface roughness in units of μm. This equation is only valid within the limits of surface roughness that were encountered for Tests 1 to 4 (131 to 165 μm). However, although the observed correlation is based on only four data points, it suggests a logical relationship that is worthy of further consideration in future research. The procedure was not applied to Specimens 5 to 8 because their energy dissipation was limited by the observed delamination, which is an altogether different failure mode whose physical behavior could only have been captured by other types of measurements.

Conclusions

Cyclic inelastic testing was performed to determine if the hysteretic energy dissipation capacity of corroded steel could be related to measured surface roughness and thickness of the corroded surface. In support of those tests, a preliminary set of monotonic tests were conducted using simple tension coupons having corroded surfaces to compare the effectiveness of the various methods considered to measure thickness. This was assessed by comparing results from finite element models having various resolutions (and thickness mapping) against experimentally-obtained monotonic force displacement curves of the corroded steel.

Results from coupons tested in this study suggest that assessing the strength of rusted members by machining a smooth coupon from steel extracted from an existing corroded structure, and only using the resulting yield and ultimate strength values in otherwise standard multilinear monotonic models, may be an unconservative approach. A more extensive data set would be required to quantify this level of unconservatism, both generally and in terms of various parameters dependent on corrosion-related characteristics, but the preliminary results obtained in this study suggest that the unconservatism could be on the order of 25%. It also was found that grid spacing for thickness mapping, within the range considered in this study, did not have a significant effect upon the accuracy of the analytical finite element model's prediction of the experimentally obtained force-displacement curves, and that the results were effectively insensitive to the various methods considered to measure thickness. This provided valuable insights needed prior to measuring thickness of the specimens subjected to cyclic testing.

Results from cycling tests show that: (1) rusted steel can exhibit a significant hysteretic energy capacity; (2) a linear relationship exists between the total dissipated energy normalized by mean thickness, and the mean 10-point-height of irregularities and; (3) increases in roughness correspond to decreases in the magnitude of total normalized energy dissipated before complete failure.

The research results presented in this paper have identified key parameters that need to be considered, important trends in behavior, and some quantification of these trends that set the direction for future research to validate and expand the range of applicability of those results. However, qualitative observation of the experimentally obtained hysteretic curves suggests that steel rusted to the severity considered in this study may still have sufficient ductility to provide adequate seismic performance.

References

AISC. (1953). "Iron and steel beams–1873 to 1952 (AISC)." Chicago.

AISC. (2010). "AISC 341-10, seismic provisions." Chicago.

Albrecht, P., and Simon, S. (1981). "Fatigue notch factors for structural details." *J. Struct. Eng.*, 107(7), 1279–1296.

ANSYS [Computer software]. ANSYS Incorporated, Canonsburg, PA.

ASTM. (1991). "Standard test methods of tension testing metallic materials." *ASTM E8-91*, West Conshohocken, PA.

ASTM. (1999). "Standard practice for preparing, cleaning and evaluating corrosion test specimens." *ASTM G1-90*, West Conshohocken, PA.

Bill, R. C. (1982). "A review of factors that influence fretting wear, in materials evaluation under fretting conditions." *STP 780*, ASTM, West Conshohocken, PA, 178–179.

Bruneau, M., Uang, C. M., and Sabelli, R. (2011). *Ductile design of steel structures*, 2nd Ed., McGraw-Hill, New York, 921.

Bruneau, M., and Zahrai, S. (1998). "Some observations on the effect of severe corrosion on cyclic ductility of steel." Ottawa-Carleton Earthquake Engineering Research Center, Ottawa.

Burke, S. (2002). "An experimental study on the non-destructive evaluation of corroded bridge steel." M.Sc. thesis, Dept. of Civil Engineering, Univ. of Ottawa, Ottawa.

Burke, S. J., and Bruneau, M. (2002). "An experimental study on the non-destructive evaluation of corroded bridge steel." *Rep. OCEERC 02-30*, Ottawa-Carleton Earthquake Engineering Research Center, Univ. of Ottawa, Ottawa, Canada, 298.

Fisher, J. W., Yen, B. T., and Wang, D. (1991). "Corrosion and its influence on strength of steel bridge members." *Transp. Res. Rec.*, 1290, 211–219.

Fitgerald, R. W. (1967). *Strength of materials*, Don Mills, Canada, 306–307.

Gucuyen, E., and Erdem, R. T. (2014). "Corrosion effects on structural behaviour of jacket type offshore structures." *Građevinar*, 66(11), 981–986.

Kayser, J. R., Malinski, T., and Nowak, A. S. (1987). "Corrosion damage models for steel girder bridges." *Proc., Effects of Damage and Redundancy on Structural Performance*, ASCE, Reston, VA, 9–22.

Kayser, J. R., and Nowak, A. S. (1989). "Capacity loss due to corrosion in steel-girder bridges." *J. Struct. Eng.*, 10.1061/(ASCE)0733-9445(1989)115:6(1525), 1525–1537.

Kulicki, J. M., Prucz, Z., Sorgenfrei, D. F., Mertz, D. R., and Young, W. T. (1990). "Guidelines for evaluating corrosion effects in existing steel bridges." *NCHRP Rep. No. 333*, Transportation Research Board, National Research Council, Washington, DC.

Nakai, T., Matsushita, H., and Yamamoto, N. (2005). "Effect of pitting corrosion on local strength of hold frames of bulk carriers (2nd Report)—Lateral-distortional buckling and local face buckling." *Mar. Struct.*, 17(8), 612–641.

Nakai, T., Matsushita, H., and Yamamoto, N. (2006). "Effect of pitting corrosion on strength of web plates subjected to patch loading." *Thin-Walled Struct.*, 44(1), 10–19.

Paik, J. K., Lee, J. M., and Ko, M. J. (2004). "Ultimate shear strength of plate elements with pit corrosion wastage." *Thin-Walled Struct.*, 42(8), 1161–1176.

Rajabipour, A., and Melchers, R. E. (2013). "A numerical study of damage caused by combined pitting corrosion and axial stress in steel pipes." *Corros. Sci.*, 76, 292–301.

Testex Corporation. (1999). "Burnishing tool and replica tape." Newark.

Yu, W., Karr, D. G., and Vargas, P. M. (2012). "Corrosion effects on reliability of flat plates in tension." *J. Offshore Mech. Arct. Eng.*, 134(2), 021404.